Pure Appl. Geophys. 176 (2019), 3769–3786

https://doi.org/10.1007/s00024-019-02140-4

Pure and Applied Geophysics

Application of Singular Spectrum Analysis for Investigating Chaos in Sea Surface Temperature

Swarnali Majumder[1] and Partha Pratim Kanjilal[2]

Abstract—The goal of this study is to explore the chaotic behavior of sea surface temperature (SST) in the Indian Ocean and in the equatorial Pacific Ocean. The SST time series is analyzed for Bay of Bengal, Arabian Sea and South Indian Ocean as well as for two extreme phenomena: El Niño and Indian Ocean Dipole (IOD). The analysis is based on Singular spectrum analysis, and singular value decomposition (SVD). Our analysis reveals that the dynamics of SST is chaotic in varying degrees in all the studied cases, since Lyapunov exponent, an indicator of chaoticity, is positive in each case. To study the degree of predictability of these SST series, we search for embedded periodic component(s) using two different approaches: Orthogonal functions extracted from the Singular spectrum analysis and Periodicity spectrum analysis based on SVD. Both the methods reveal presence of a strong periodic component(s) for the SST signals in the Arabian Sea, Bay of Bengal and South Indian Ocean, whereas no periodicity is found for El Niño and IOD. Therefore, it can be concluded that the dynamics of SST is more complex in the El Niño and IOD region compared to Bay of Bengal, Arabian Sea and South Indian Ocean; hence it is much more difficult to predict El Niño and IOD.

Key words: Sea surface temperature, chaos, singular spectrum analysis, singular value decomposition, El Niño, Indian Ocean Dipole.

1. Introduction

Sea surface temperature (SST) is one of the key indicators of oceanic and atmospheric variability and hence predictability of SST is of particular interest for proper understanding of the changing oceanic conditions. In the present work, we study the dynamics associated with the SST time series at Arabian Sea, Bay of Bengal and South Indian Ocean as well as for two extreme phenomena: El Niño and Indian Ocean Dipole (IOD). El Niño involves prolonged warming in the equatorial Pacific Ocean SST, compared to the average value. IOD is another complex phenomena in which the Western part of Indian Ocean becomes alternately warmer and cooler than the Eastern part (Saji et al. 1999). It is difficult to forecast El Niño (Jin et al. 2008; Yu et al. 2012). There remains considerable uncertainty in IOD prediction too (Shi et al. 2012). Although several studies have shown variability of SST in the Arabian Sea, Bay of Bengal and South Indian Ocean (Behera and Yamagata 2001; Waliser et al. 2003; Jochum and Murtugudde 2005), the SST time series of these regions do not show any sudden change like the indices of El Niño and IOD. The present work attempts to understand the distinction between the dynamics of the extreme phenomena of El Niño and IOD from the dynamics of usual SST in the Arabian Sea, Bay of Bengal and South Indian Ocean.

The physical processes of El Niño and IOD can be described as follows. Under normal climatic conditions, the atmospheric pressure of the Eastern Pacific is higher than the west. This difference of atmospheric pressure generates the tropical easterlies and drives the Eastern Pacific Ocean current westward. The westbound ocean currents are heated by the sun and gathers in the central and Western Pacific. In the Eastern Pacific, the low temperature sea water in the deep ocean flows up to replace the westbound ocean currents. During El Niño, the atmospheric pressure of the Eastern Pacific decreases and the pressure in the west increases. This sudden difference in atmospheric pressure reduces the strength of the tropical

Electronic supplementary material The online version of this article (https://doi.org/10.1007/s00024-019-02140-4) contains supplementary material, which is available to authorized users.

[1] Indian National Centre for Ocean Information Services, Ocean Valley, Pragathi Nagar, Nizampet, Hyderabad 500 090, India. E-mail: swarnali.majumder48@gmail.com

[2] FINRA, New York, USA. E-mail: parthakanjilal@yahoo.com

easterlies. So the ocean current of the Eastern Pacific flows towards east and accumulates in the Eastern Pacific region. SST rises in this region by heating from the sun. This in turn results in higher Eastern Pacific temperature. In the phenomenon of IOD, a positive IOD results when Eastern equatorial Indian Ocean is cooler than normal SST and the Western tropical Indian Ocean is warmer than normal SST. A negative IOD is characterized by warmer than normal SST in the Eastern equatorial Indian Ocean and cooler than normal SST in the Western tropical Indian Ocean. During positive IOD, equatorial surface winds, which in a normal condition blows towards east, weakens and blows towards west. Rainfall increases over the Western Indian Ocean, while over the Indonesia and Australia it decreases, resulting in drought. During negative IOD, westerly winds intensify along the equator. Eastern Indian Ocean is flooded whereas dried condition is observed in the Western Indian Ocean. Since several oceanic and atmospheric processes are intertwined in the mechanisms of El Niño and IOD, intuitively these are complex systems.

The physical reasons behind the nonlinearity of SST is its interannual and longer timescale variability due to the various atmospheric and oceanic processes and the coupled ocean–atmosphere interaction like El Niño. On the oceanic side, heat transport by currents, vertical mixing and boundary layer depth influence SST. On the atmospheric side, significant changes in the turbulent and radiative energy fluxes at the air–sea interface and the local wind-driven Ekman currents cause variation in SST (Alexander and Scott 2008; Deser et al. 2010). In support of the linearity of SST one can argue that linear models produce forecasts as good as fully nonlinear GCMs (Newman and Sardeshmukh 2017), and apparently nonlinear models do not improve over linear models on Niño 3.4 forecasts (Chen et al. 2016). In any case, the accurate forecasting of SST is a challenging task (Li and Xie 2012). Proper understanding of the dynamics of SST can help produce reliable forecasts. In this study, SST time series is explored in monthly time scale. There has been several studies on the analysis and modeling of the SST series as follows.

1.1. El Niño Series

It has been shown that ENSO is a linearly stable multivariate system driven by Gaussian noise in interannual time scale (Penland and Sardeshmukh 1995; Kleeman and Moore 1997; Thompson and Battisti 2000). On the other hand, several studies have been devoted to identifying nonlinearity and chaos in the process of El Niño. Conceptual models for El Niño include nonlinear oscillators (Munnich et al. 1991; Neelin et al. 1998) or fully chaotic systems (Tziperman et al. 1994; Stone et al. 1998). In the above studies, either the experiment is conducted with a coupled atmosphere–ocean model to simulate El Niño, or some nonlinear equation is proposed to show the chaotic nature of El Niño. Jolliffe (2002) analyzed the time series of El Niño variability by using Singular spectrum analysis, but did not address its chaotic property.

1.2. IOD Series

Researchers have differing opinions regarding the nature of the dynamics of the Indian Ocean SST, because of its complexity compared to that of the tropical Pacific. Some study has shown that SST variability in the Indian Ocean can be compared to a spatial first order autoregressive process (Dommenget 2007). Penland (1996) showed that Indo Pacific SST anomalies could be represented as a stable linear process driven by spatially coherent stochastic forcing. However, several researchers believe that IOD, the dominant mode of the climatic variability in the Indian Ocean, is a chaotic process (Majumder et al. 2019) and grown by complex ocean–atmosphere interaction in the Indian Ocean (Anderson 1999; Saji et al. 1999; Yamagata et al. 2004).

1.3. Arabian Sea, Bay of Bengal and South Indian Ocean Series

Rao and Sivakumar (2000) have shown periodicity in SST of the Arabian Sea, Bay of Bengal and South Indian Ocean. Tourre and White (1995) showed that between one-third and one-half of the observed interannual variability in the Indian Ocean is a result of El Niño. There is a climate mode in the

Southern Indian Ocean known as Indian Ocean subtropical dipole (IOSD), which contributes substantial variability in the South Indian Ocean (Behera and Yamagata 2001). Waliser et al. (2003) found that in the central equatorial Indian Ocean and the Bay of Bengal, the rectification of the Madden–Julian oscillation onto the SST produces interannual SST anomalies of about 0.3°K, which is comparable to the observed interannual variability. Jochum and Murtugudde (2005) explained how eddies contribute to the interannual variability in the Arabian Sea. The eddies make a net contribution to the mixed layer heat budget. As the generating processes are unstable and nonlinear, this contribution will vary and the SST will be different from year to year, even under climatological forcing. However, the study of the chaotic properties of SST of these regions has remained unexplored.

In this study, Singular spectrum analysis is applied for analyzing the dynamics of SST at each of the Nino 3.4 region, the IOD region, and the Bay of Bengal, the Arabian Sea and the South Indian Ocean regions separately. The key findings of this work are (1) the dynamics of SST is shown to be chaotic in all of the studied regions; (2) a method based on singular spectrum analysis is proposed, which indicates the presence of the nonlinear components in the SST signals of the Arabian Sea, Bay of Bengal and South Indian Ocean; (3) it is shown that the dynamical system of SST does not contain any periodicity in the El Niño and the IOD regions, whereas SST series has distinct embedded periodicity in case of Bay of Bengal, Arabian Sea and South Indian Ocean, rendering the former more complex and less predictable than the latter.

The paper is organized as follows. The data and their sources used in this study are detailed in Sect. 2. The concept of singular spectrum analysis is introduced in Sect. 3. Section 4 describes the formation of State space diagram and its application to the different SST series. The detection of nonlinearity follows in Sect. 5. Section 6 describes the concepts of periodicity detection using orthogonal functions and the Periodicity spectrum analysis, along with the results. The discussions and conclusions appear in Sect. 7.

2. The Data

Monthly mean of SST data used in this study is taken from Hadley Centre, which is available at (http://www.metoffice.gov.uk/hadobs/hadisst/) (downloaded on 24.01.17). The Hadley Centre SST data are obtained from the Met Office Marine Data Bank (MDB), which from 1982 onwards also includes data received through the Global Telecommunications System (GTS). For enhancing data coverage, monthly median SSTs for 1871–1995 from the Comprehensive Ocean–Atmosphere Data Set (COADS) (now ICOADS) were also used where there were no MDB data. The details of this data set are given in Rayner et al. (2003). In this study, data for the period from January 1871 to December 2014 are used. Monthly climatology is subtracted from the observed data for creating SST anomaly.

Nino 3.4 index (the average of SST over the region 5°N–5°S and 170°–120°W) is used for measuring the intensity of El Niño. Nino 3.4 anomaly is considered from January 1950 to December 2014. The data are downloaded from (http://www.cpc.ncep.noaa.gov/products/analysis_monitoring/ensostuff/ensoyears.shtml) (downloaded on 24.01.17). It is 3 month running mean of SST anomalies in the Niño 3.4 region (5°N–5°S, 120°–170°W), based on centered 30-year base periods updated every 5 years. For constructing Nino 3.4 index, Extended Reconstructed Sea Surface Temperature (ERSST) (version 4) is used as the SST data set. ERSST data set is a global monthly SST data set derived from the International Comprehensive Ocean–Atmosphere Data set (ICOADS). It is produced on a $2° \times 2°$ grid with spatial completeness enhanced using statistical methods. The details of this SST data are given in Huang et al. 2014.

Dipole Mode Index (DMI) is the measure of the intensity of IOD. DMI is represented by anomalous SST gradient between the western equatorial Indian Ocean (50°E–70°E and 10°S–10°N) and the South Eastern equatorial Indian Ocean (90°E–110°E and 10°S–0°N). Here DMI data are downloaded from (http://www.jamstec.go.jp/frcgc/research/d1/iod/HTML/Dipole%20Mode%20Index.html) (downloaded on 24.01.17). The SST data of Hadley Centre are used to compute this product. DMI is

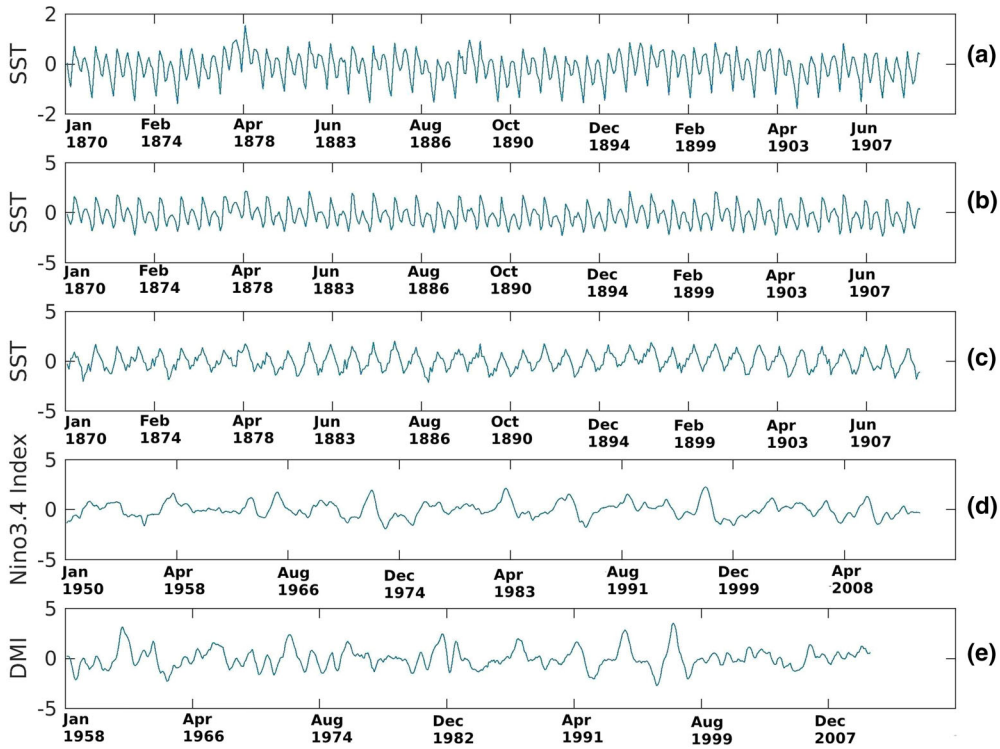

Figure 1
Time series of **a** SST in the Arabian Sea, **b** SST in the Bay of Bengal, **c** SST in the South Indian Ocean, **d** Nino 3.4 Index, **e** Dipole Mode Index (IOD)

considered from January 1958 to December 2010. Figure 1 shows the time series of SST anomalies at different regions.

3. *Singular Spectrum Analysis*

Singular spectrum analysis (SSA) is popularly used for investigating the non-linear behavior of a complex system (Golyandina et al. 2001; Jolliffe 2002). It is a non-model oriented technique, which exhibits a compact representation of the data. This method can be used as a tool to filter any data, isolate a trend or separate an oscillatory compound hidden in a noisy series. In a way it is a standard tool in the analysis of climatic, meteorological and geophysical time series (Yiou et al. 1996; Hannachi et al. 2007).

The implementation of SSA involves the following two steps. First the data series is configured into a trajectory matrix as follows. Let the time series $\{x\} = (x_0, x_1, \ldots, x_{N-1})$ and the time delay vectors $Xj = (x_{j-1}, x_j, x_{j+1}, \ldots, x_{j+L-2})^{\mathrm{T}}$, $j = 1, 2, \ldots, \mathrm{K}$, where K is the 'embedding dimension' and $\mathrm{L} = \mathrm{N} - \mathrm{K} + 1$. As shown below, the trajectory matrix is given by $\boldsymbol{X} = [X1: X2 \ldots : XK]$. The trajectory matrix $\boldsymbol{X}$ is a Hankel matrix. The embedding procedure maps the original time series to a sequence of multidimensional time delay vectors (Takens 1981). In this type of matrix formation, SSA incorporates temporal correlation:

$$\boldsymbol{X} = \begin{bmatrix} x(0) & x(1) & \ldots & x(K-1) \\ x(1) & x(2) & \ldots & x(K) \\ \ldots & \ldots & \ldots & \ldots \\ x(N-K) & x(N-K+1) & \ldots & x(N-1) \end{bmatrix}.$$

The second step is the singular value decomposition (SVD) of the matrix $\boldsymbol{X}$. SVD decomposes $\boldsymbol{X}$ as $\boldsymbol{X} = \boldsymbol{U}\boldsymbol{S}\boldsymbol{V}^{\mathrm{T}}$, where $\boldsymbol{U}$ is an Lx L orthogonal matrix, $\boldsymbol{S}$ is a $\mathrm{L} \times K$ dimensional diagonal matrix and $\boldsymbol{V}$ is a

K × K orthogonal matrix. $\boldsymbol{U}$ represents the eigen vectors of $\boldsymbol{XX}^{\mathrm{T}}$ and $\boldsymbol{V}$, the eigen vectors of $\boldsymbol{X}^{T}\boldsymbol{X}$. The diagonal elements of $\boldsymbol{S}$ are the singular values of $\mathbf{X}$. The column vectors of $\boldsymbol{U}$: ($U1$, $U2$,…,UK) are the 'empirical orthogonal functions' (EOFs). The idea behind SVD is that most of the variance (or power) is contained within the first few components. Diagonal elements of $\boldsymbol{S}$: $\{s_1, s_2, \ldots, s_K\}$ are arranged in a non-increasing order, i.e. $s_1 \geq s_2 \geq s_3 \ \ldots \geq s_K$. It is assumed that the diagonal elements with lower magnitude are associated with the noise in the signal. So the negligibly small singular values are assigned to zero and the leading significant values, say $\{s_1, s_2, s_3, \ldots, s_p\}$ are considered, where $p <$ K. Now let us call this new matrix as $\boldsymbol{S}'$ and consider reconstructed relationship $\boldsymbol{X}' = \boldsymbol{U}'\boldsymbol{S}'\boldsymbol{V}'^{T}$. The reconstructed time series formed by joining the successive rows of $\boldsymbol{X}'$ is expected to be relatively free from noise.

In the next section, SSA method is used for exploring the dynamics of SST in the different regions of the Indian Ocean and Nino 3.4 and IOD regions.

4. State Space Diagram Reconstruction and Results

The reconstruction of the state space diagram is the first step for the analysis of a time series in terms of dynamical systems theory (Casdagli et al. 1991; Takens 1981). Since the dynamics of the system is unknown, one cannot reconstruct the original attractor from the observed time series. Instead, an embedding space is created where one can reconstruct an attractor from the time series that preserves the invariant characteristics of the original unknown attractors. The trajectories of the state space diagram describe the evolution of the system from some initial state (assumed to be known) and convey some information about the dynamical system. Differences in state space diagram indicate that the corresponding dynamical systems are different from each other.

Broomhead and King (1986) initiated the application of Singular spectrum analysis for reconstructing attractor from a noisy data. As discussed in the previous section, a Hankel matrix, say $\boldsymbol{X}$, is created from the time series of SST anomaly. Here the embedding dimension K is determined empirically for each time series. SVD is performed on $\boldsymbol{X}$ and the first column of $\boldsymbol{U}$, say $U1$, is used for extracting the state space diagram. The state space diagram can be reconstructed by plotting $U1(t)$ vs. $U1(t + d)$, where t is any time step and d is the time lag. d is the minimum number of geometric co-ordinates needed to complete the system dynamics. In this study, state space diagram is created by plotting $U1(t)$ vs. $U1(t + d)$ (Fig. 2). Here d is empirically chosen as 5, which is not a limitation. Empirically it is found out that if d is less than 5, we do not get any state space diagram. If we increase d, we still get state space diagram, however if we take high value of d, noise might contaminate the state space. Hence it is optimal to keep d as low as possible. So d is taken as 5. Figure 2a, b show the state space diagrams of the Arabian Sea and Bay of Bengal respectively. They are not strictly periodic, as in each of the cases, trajectory does not come back to the exact point from where it started. In a chaotic system, close state space trajectories will diverge, and they will never close on themselves. The same is observed in the state space diagram of South Indian Ocean (Fig. 2c), although its shape is a little different from Arabian Sea and Bay of Bengal, indicative of some differences in the embedded dynamics. The state space diagrams of Nino 3.4 Index and Dipole Mode Index (IOD) are obviously not periodic and both are apparently non-linear (Fig. 2d, e). Monthly data are required for creating state space diagrams as 3 monthly or 6 monthly data do not produce proper state space diagrams due to under sampling. For quantitative assessment of the chaos, Lyapunov exponent is computed to study the existence of chaos in each of these signals.

5. Detection of Nonlinearity Using Lyapunov Exponent

Lyapunov exponent describes the rate at which close trajectories diverge or converge in the state space diagram of a time series (Rosenstein et al. 1993). So it is a direct measure of chaos of a system and it is a measure of predictability also. Two trajectories in phase space with initial separation l_0 diverge at a rate given by $l(t) \sim l_0 e^{\lambda t}$, then λ is the

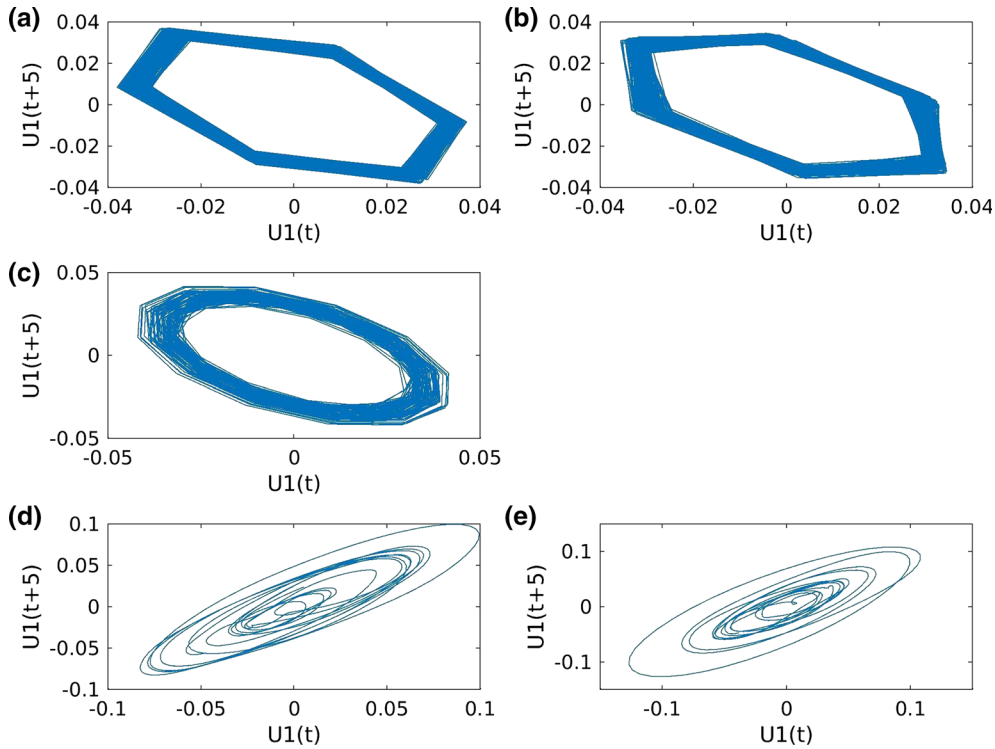

Figure 2
State space diagram of **a** SST in the Arabian Sea, **b** SST in the Bay of Bengal, **c** SST in the South Indian Ocean, **d** Nino 3.4 Index, **e** Dipole Mode Index (IOD)

Lyapunov exponent. In this study, Lyapunov exponents are obtained by using Rosenstein's method. The first step of this method is the reconstruction of the attractor from a single time series. Next nearest neighbor is computed for each point on the trajectory. The nearest neighbor, say X_j', is located by finding the point that minimizes the distance to the particular reference point, X_j. This is expressed as $d_j(O)$= min norm$(X_j - X_j')$, (minimization is over X_j'), where $d_j(O)$ is the initial distance from the jth point to its nearest neighbor, and 'norm' is the Euclidean norm. An additional constraint is that the nearest neighbors have a temporal separation greater than the mean period of the time series, i.e. abs$(j - j') >$ mean period. This allows one to consider each pair of neighbors as nearby initial conditions for different trajectories. The largest Lyapunov exponent is then estimated as the mean rate of separation of the nearest neighbors. Since sensitive dependence on initial condition is a significant property of chaotic dynamics, a positive Lyapunov exponent is an indication of chaos in a system. One limitation of this technique is that Lyapunov exponent cannot distinguish chaos from noise. So noise reduction is an important step before computing Lyapunov exponent (Dammig and Mitschke 1993; Eckmann and Ruelle 1992). Hence, in this study, SSA method is used to reconstruct the noise free signal before computing Lyapunov exponent. For example, Fig. 3 shows the singular values of Nino 3.4 index. A drop down is noticed after the 16th mode. Hence the first 16 orthogonal modes are assumed to constitute the signal and the rest are assumed to be noise; so to reconstruct the data the first 16 diagonal values of the diagonal matrix are used and the other values are assigned to 0 (as explained in Sect. 3). With this new diagonal matrix, say, $\boldsymbol{S}''$, the filtered signal is produced. There is a limitation of this technique. The last few modes

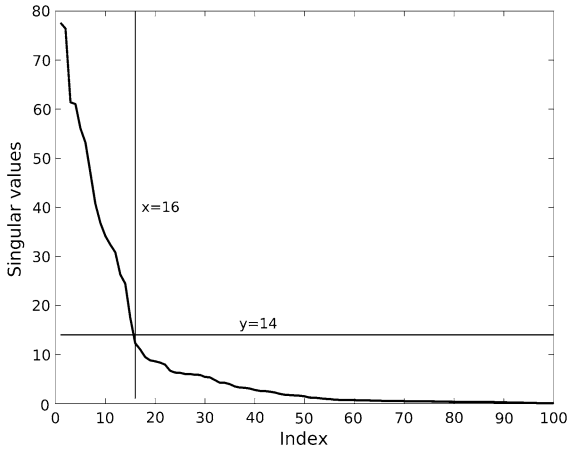

Figure 3
Singular values of Nino 3.4 index

associated with the higher singular values represent noise in SVD. Since the cut off singular value is selected arbitrarily, this method does not remove noise completely. Yet this method helps in capturing the essence of the signal. Since the first few orthogonal modes are considered after performing SVD, noise is partially removed in this technique. The Lyapunov exponent is calculated for this filtered signal using the Tiseanpath package (Hegger and Kantz 1999). Each signal is partitioned in two parts (say, 'period 1' and 'period 2') based on its time period. For Nino 3.4 Index, period 1 is considered from 1950 to 1982 and period 2 is considered from 1983 to 2014. For DMI, period 1 is considered from 1958 to 1984 and period 2 is considered from 1985 to 2010. In case of SST signals in the Arabian sea, Bay of Bengal and South Indian Ocean, period 1 is taken from 1871 to 1943 and period 2 is taken from 1944 to 2014. Lyapunov exponent is calculated for all of the years as well as for period 1 and period 2. Table 1 shows that Lyapunov exponent is positive in all cases. We have tested cases with variations in the number of retained modes (16–20 retained modes) and the Lyapunov exponent is positive in all cases. As Lyapunov exponent is positive, all of these signals are detected to be chaotic. At the same time, the distinct difference between the magnitudes of the Lyapunov exponent necessitates further analysis; so we proceed with periodicity detection for additional understanding of their underlying dynamics.

Table 1

Lyapunov exponent of the SST signals

Time Series	All years	Period 1	Period 2
Nino 3.4 Index	0.3	0.28	0.3
Dipole Mode Index	0.32	0.3	0.31
Arabian Sea	0.1	0.08	0.09
Bay of Bengal	0.15	0.13	0.14
South Indian Ocean	0.15	0.12	0.14

6. Detection of Periodicity and Results

The rationale for the search for periodicity embedded in a SST series is that the presence of periodicity can be intuitively linked with the predictability of the series. We search periodicity by two different approaches: using EOFs and by using periodicity spectrum.

6.1. Detection of Periodicity Using Orthogonal Functions

Empirical orthogonal function can explain the variability as well as the inherent periodicity of a signal (Golyandina et al. 2001). Figures 4 and 5 show the 1st to 6th EOFs ($U1$, $U2$, $U3$, $U4$, $U5$, $U6$) of Nino 3.4 index and DMI respectively. In both of the cases, no periodicity is observed in any EOF. It has been shown that the Tropical Pacific SST anomalies are phase-locked to the annual cycle (Sarachik and Cane 2010; Clarke 2008). In SSA technique, the first EOF represents the trend of the signal and the consecutive few modes represent the dominant components the signal. There is no dominant periodic component in Nino 3.4 index. So it is not captured by the first few modes of EOF. This does not mean that there is no periodic orbit in the system. There can be local periodicity in the system. P-spectrum shows the globally stable periodic orbit. Absence of periodic orbit in p-spectrum does not indicate that there is no local periodicity in the system. There still can be periodic orbit in the system which is not globally stable. $U1$, $U2$, $U4$ and $U5$ of the Arabian Sea and the Bay of Bengal are periodic as shown in Figs. 6 and 7, respectively. $U1$ and $U2$ represent 6 monthly periodicity and $U4$ and $U5$ represent the 1 yearly

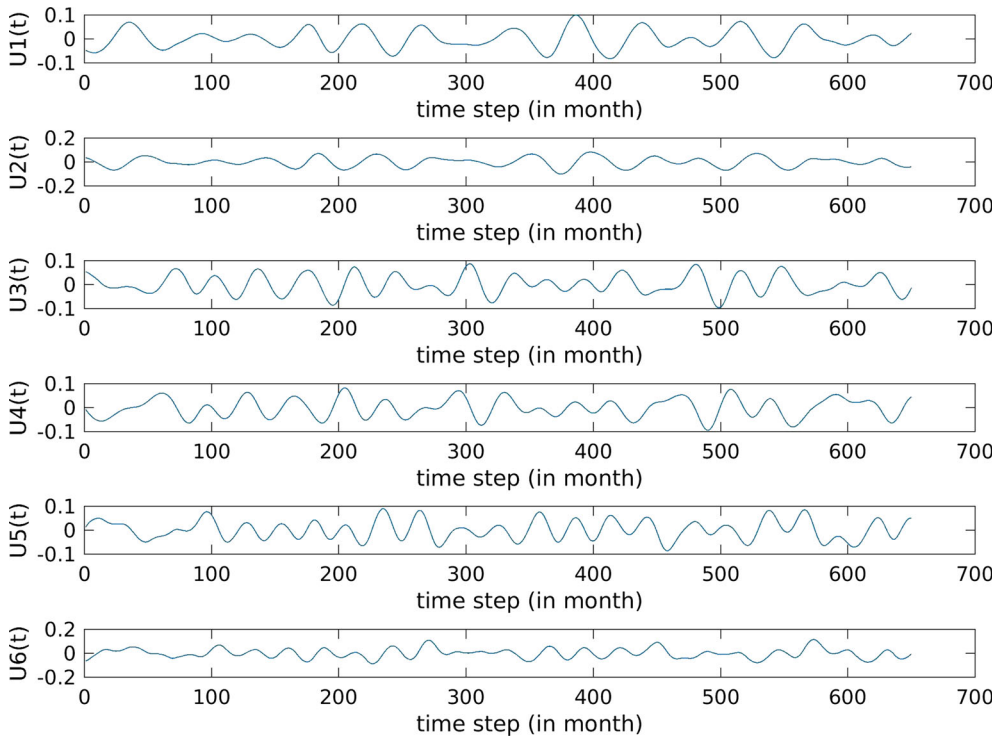

Figure 4
1st, 2nd, 3rd, 4th, 5th and 6th columns of U matrix of Nino 3.4 index

periodicity. For the South Indian Ocean, $U1$ and $U2$ are periodic with 1 yearly periodicity (Fig. 8). The physical understanding of the SST process corroborates these findings. In the South Indian Ocean, only the movement of the sun influences SST. In the North Indian Ocean, both the sun and the monsoon wind influences the SST. Rao and Sivakumar (2000) showed that the heat content of the near-surface layers of the Arabian Sea and the Bay of Bengal registers excessive drops with the onset and progress of the summer monsoon. Under the influence of direct solar heating during February to May the seasonal buildup of the warm pool attains its maximum amplitude in May, with its core in the Southeastern Arabian Sea and Southwestern Bay of Bengal. The onset and sway of the summer monsoon during June to September progressively cools the near-surface layers of the ocean. Hence, in the North Indian Ocean, periodicity is observed at 6 months as well as 1 year. In the South Indian Ocean, only yearly periodicity is observed as SST is not influenced by monsoon in this region. In our analysis, the excursions of $U3$ stands out as different; we conjecture that $U3$ represents nonlinearity and is not noise as as noisy components are usually associated with the higher EOFs (or smaller singular values) in the SSA method.

Although some studies have shown empirical interpretation of the orthogonal components obtained from SSA related techniques (Kondragunta and Gruber 1997; Saji et al. 1999), there is no certainty or theoretical basis for such interpretations because the physical modes are not necessarily orthogonal as captured through SSA (Dommenget and Latif 2002; Jolliffe 2002). Features can be mixed between orthogonal components if their corresponding eigen values are similar. So we cannot be certain about any physical representation of the components of El Niño and IOD signals. However, SSA technique is a useful tool to extract dynamical structure, e.g., trends, oscillations, and propagating structures etc. (Golyandina et al. 2001; Plaut and Vautard 1994). Hence we can be certain about the periodic components

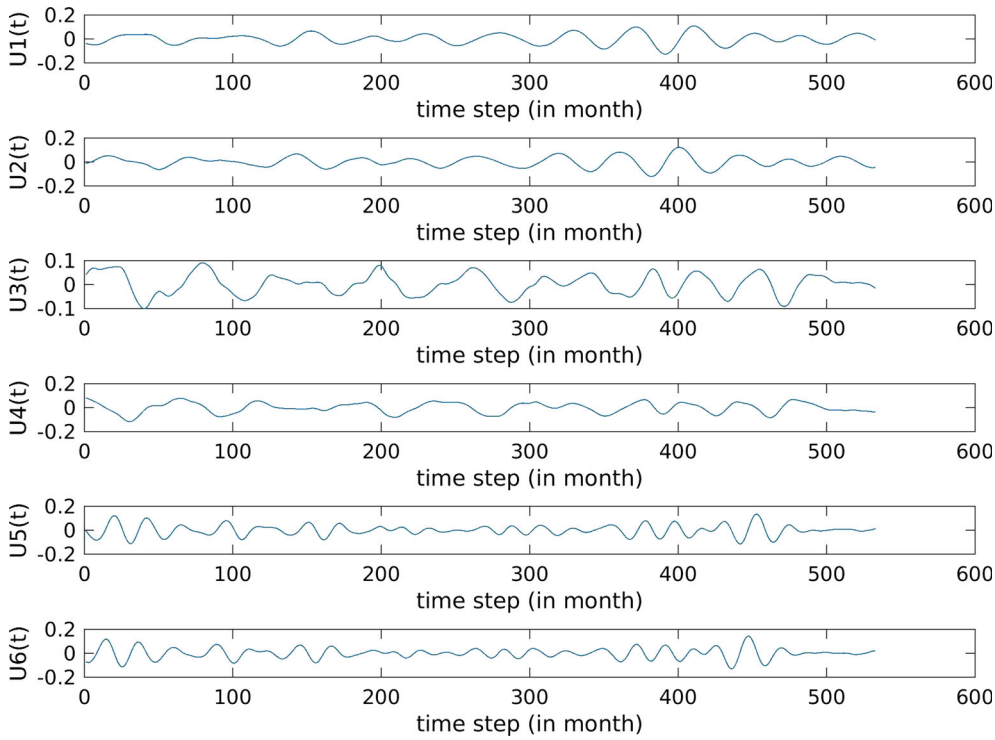

Figure 5
1st, 2nd, 3rd, 4th, 5th and 6th columns of U matrix of Dipole Mode Index

obtained by this method in the Arabian Sea, Bay of Bengal and South Indian Ocean.

In order to estimate the amount of the periodicity contained in the signals, we consider the singular value spectrum constituting the singular values (s_i) of $\boldsymbol{S}$. The normalized singular value (n_i) is computed by the formula $n_i = s_i^2/(\sum_i s_i^2)$, where i varies from 1 to K. The magnitude of a normalized singular value n_i is indicative of the variance of the corresponding EOF Ui (Cattell 1966). In the Bay of Bengal and Arabian Sea, $U1$ and $U2$ show 6-monthly periodicity, $U3$ shows nonlinearity and $U4$ and $U5$ show 1-yearly periodicity. In the Bay of Bengal, normalized singular values are 0.25, 0.25, 0.14, 0.06 and 0.06 corresponding to $U1$, $U2$, $U3$, $U4$ and $U5$. So the signal represents 50% 6-monthly periodicity 14% nonlinearity and 12% 1-yearly periodicity. In the Arabian Sea, the corresponding normalized singular values are 0.26, 0.24, 0.14, 0.06 and 0.05, representing 50% 6-monthly periodicity, 14% nonlinearity and 11% 1-yearly periodicity. In the South Indian Ocean, normalized singular values are 0.35, 0.35 and 0.05 corresponding to $U1$, $U2$ and $U3$, where $U1$ and $U2$ show 1-yearly periodicity and $U3$ shows nonlinearity. Therefore, this signal represents 70% 1-yearly periodicity and 5% nonlinearity. This empirical approach shows that Bay of Bengal and Arabian Sea have comparatively stronger nonlinear components than South Indian Ocean. The other components are ignored as they exhibit relatively less variability of less than 3% (Table 2).

Next, we address the question: can the relatively periodic SST series be predicted using the individually predicted orthogonal functions? The concept can be described by the following procedure: (a) model the series of elements in the individual $N - k + 1$ long Ui column vectors of $\boldsymbol{U}$ as an autoregressive process, (b) use the model to produce 1-step ahead prediction element ui'_{N-k}, (c) use this prediction to construct the K-long vector: $ui'_{N-K}\boldsymbol{S}(i,i)Vi^T$, where $\boldsymbol{S}(i,i)$ is the ith singular value and Vi^T is the ith row of $\boldsymbol{V}^T$. (d) add the vectors generated at the last step for

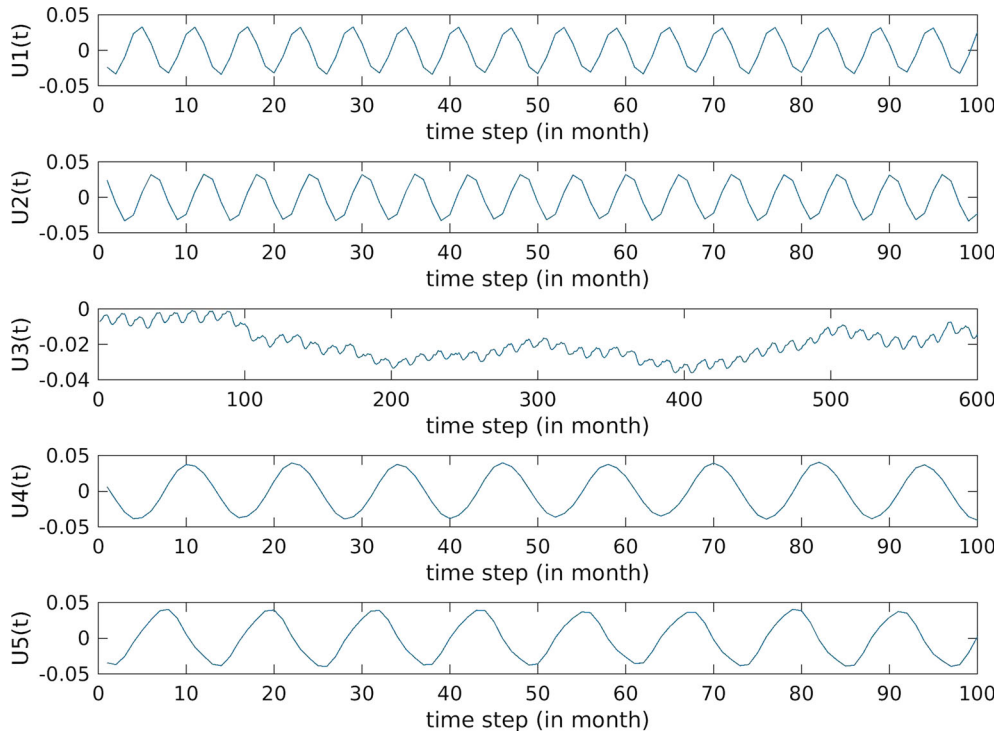

Figure 6
1st, 2nd, 3rd, 4th and 5th columns of U matrix ($U1$, $U2$, $U3$, $U4$, $U5$) of the SST signal in the Arabian Sea

i =1, 2 etc. to form the composite prediction vector $(x_{N-K}, x_{N-K+1}, \ldots, x_{N-1})'$, which is the reconstructed signal. With reference to Sect. 3, here the assumption is that for $L \times K$ matrix $\boldsymbol{X}$ and period length K, the periodic pattern Vi^T remains unchanged in the $L + 1$th period. In the case of South Indian Ocean, we consider the first two columns of $\boldsymbol{U}$, i.e. $U1$ and $U2$. So the autoregression model stands as $u1_{n+1} = a_1 u1_n + a_2 u1_{n-1} + a_3 u1_{n-2} + a_4 + e_n$, where n varies from 3 to (N − K − 1); a_1, a_2 etc. parameters are estimated using least squares estimation and e_n is white noise. The AR model is used to generate the prediction $u1'_{N-K}$. $U2$ is also modeled similarly and prediction $u2'_{N-K}$ is produced. So $(u1'_{N-K}\boldsymbol{S}(1,1)V1^T + u2'_{N-K}\boldsymbol{S}(2,2)V2^T)$ yields the predicted or reconstructed signal $(x_{N-K}, x_{N-K+1}, \ldots, x_{N-1})'$. Figure 9 shows that the reconstructed signal (dashed line) captures the cyclical trend of the original signal (solid line). The procedure is repeated for Arabian Sea and Bay of Bengal, where $U1$, $U2$, $U4$ and $U5$ components of $\boldsymbol{U}$ matrix are considered, which are individually modeled and extended for signal reconstruction. In both these cases, the reconstructed signal captures the trend of the original series as shown in Figs. 10 and 11. In the Arabian Sea, standard deviation (STD) of SST is 0.5 and root mean square error (RMSE) between the actual SST and reconstructed SST is 0.65. In the Bay of Bengal RMSE is 0.5, whereas STD is 0.6. In the South Indian Ocean RMSE is 0.7, whereas STD is 1.1. Irrespective of the fact that all these signals are chaotic with positive Lyapunov exponents (as shown in Sect. 5), some periodic components are found in each case and the original signals can be reconstructed from those periodic components. The error in reconstructions may be attributed to the influence of nonlinear components in each of these signals. Since reasonable reconstruction is possible even without the nonlinear components, these results lead to the conclusion that the influence of non-periodic components is relatively insignificant in the three studied cases.

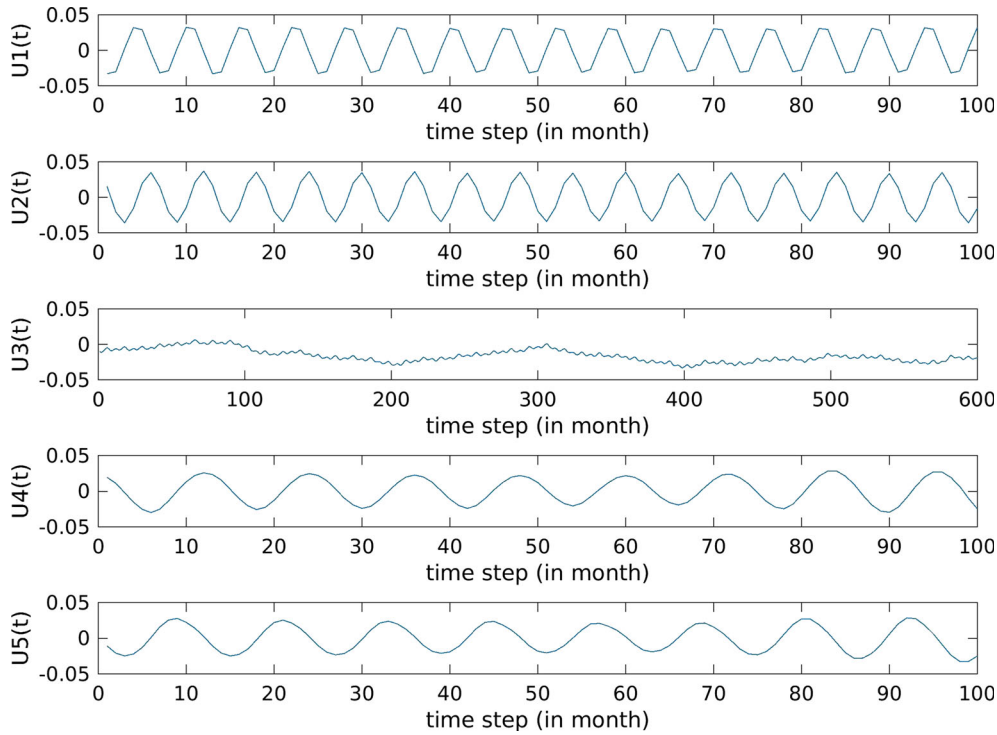

Figure 7
1st, 2nd, 3rd, 4th and 5th columns of U matrix ($U1$, $U2$, $U3$, $U4$, $U5$) of the SST signal in the Bay of Bengal

6.2. *Detection of Periodicity Using Periodicity Spectrum*

To reinforce our previous results in terms of the embedded periodicity, we compute Periodicity spectrum (or p-spectrum) for each of these signals (Kanjilal et al. 1999). Let the time series $\{x\}= (x_0, x_1, \ldots, x_{N-1})$ be configured into an $m \times n$ matrix $\boldsymbol{A_n}$:

$$\boldsymbol{A_n} = \begin{bmatrix} x(0) & x(1) & \ldots & x(n-1) \\ x(n) & x(n+1) & \ldots & x(2n-1) \\ \ldots & \ldots & \ldots & \ldots \\ x((m-1)n) & x((m-1)n+1) & \ldots & x(mn-1) \end{bmatrix}.$$

This configuration of the data matrix is different from the conventional Hankel matrix form of the trajectory matrix described in Sect. 3. In the conventional form, all the states (in sufficient embedding dimensional space) are considered. In the present case, only the states, which are n sequences apart from each other, are considered in the successive rows, with no overlapping of data elements across the rows of the matrix. The series $\{x\}$ is configured into $m \times n$ matrix $\boldsymbol{A}_n$ with varying row length n and SVD of $\boldsymbol{A}_n$ is performed. SVD decomposes $\boldsymbol{A_n}$ into three matrices $\boldsymbol{U}$, $\boldsymbol{S}$ and $\boldsymbol{V}$. The spectrum of the ratio of first two singular values s_1/s_2 vs. row length (n) is called the singular value ratio (SVR) spectrum or Periodicity spectrum (Kanjilal 1995; Kanjilal et al. 1999). If there is any periodic component of periodicity N embedded in the series $\{x\}$, Periodicity spectrum will show repetitive peaks at row lengths $n = iN$ (where i is a positive integer), and this serves as periodicity detection. A dominant first singular value for any $m \times n$ matrix $\boldsymbol{A}_n$ is indicative of the presence of a strong periodic component (of period length n) in $\{x\}$. First row of the matrix $\boldsymbol{V^T}$, say $\boldsymbol{V}1$, represents the periodic pattern of the signal.

Figures 12, 13 and 14 show the periodicity spectrum of SST in the Arabian Sea, Bay of Bengal and South Indian Ocean respectively. In each of these cases, strong peaks are observed when row lengths are 12, 24, 36 and 48, which confirms the presence of dominant periodicity of 12 (months) in these signals. Figures 15 and 16 show the Periodicity spectrum for

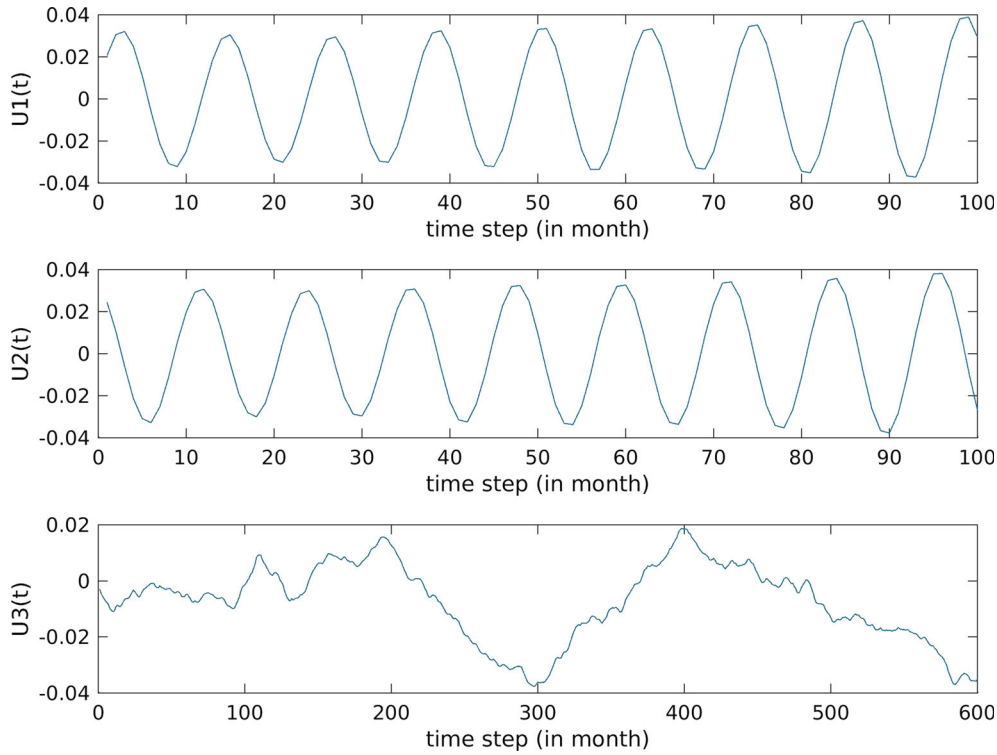

Figure 8
1st, 2nd and 3rd columns of U matrix ($U1$, $U2$, $U3$) of the SST signal in the south Indian Ocean

Table 2

The energy contained in the periodic and nonlinear components present in the SST signals of different regions

Region	6-Monthly periodic component	1-Yearly periodic component (%)	Aperiodic or non-linear component associated with $U3$ (%)
Arabian Sea	50%	11	14
Bay of Bengal	50%	12	14
South Indian Ocean	–	70	5

Nino 3.4 index and DMI, where no strong peak is observed. Since nonlinear transformation may accentuate the peaks in p-spectrum (Kanjilal et al. 1999), we apply nonlinear transformation preceding the computation of p-spectrum for these two series but still no peaks are observed. This confirms the fact that no stable periodic orbit exists in the dynamical systems of El Niño and IOD.

Here, the method of Periodicity spectrum analysis is chosen over Fourier decomposition. This is because Fourier decomposition has inherent limitation of each component being sinusoidal with constant scaling throughout; Kanjilal et al. (1999) further showed that Fourier decomposition can be misleading for periodicity detection, when noise and signal bandwidths overlap or when the constituent periodic components have overlapping frequency bands, whereas the Periodicity spectrum remains relatively unaffected.

6.3. *Computation of Residual Series and Detection of Chaos in the Indian Ocean*

Next we address the question: can the positive Lyapunov exponents in the current relatively periodic SST series be attributed to associated

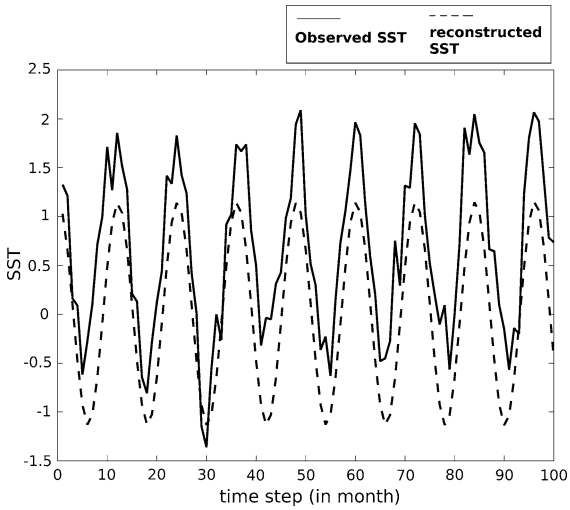

Figure 9
Observed and reconstructed SST in the South Indian Ocean

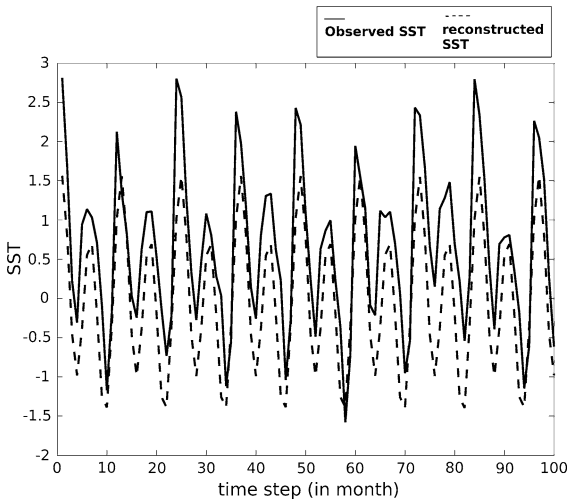

Figure 10
Observed and reconstructed SST in the Arabian Sea

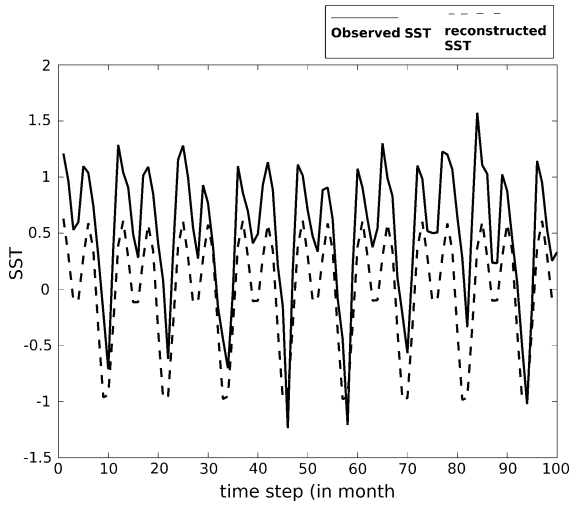

Figure 11
Observed and reconstructed SST in the Bay of Bengal

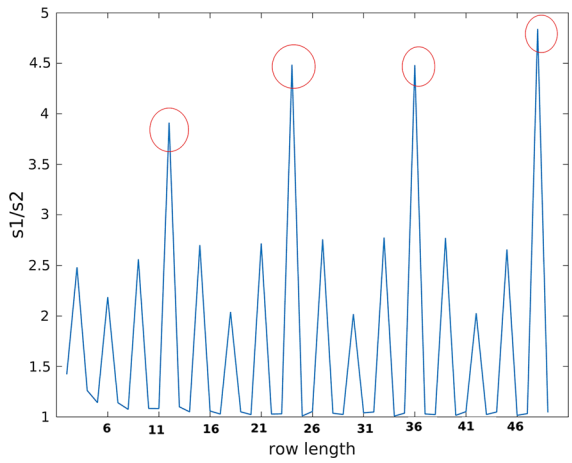

Figure 12
Periodicity spectrum of SST in the Arabian Sea

noise rather than the inherent nonlinearity? As shown in Sects. 6.1 and 6.2, strong periodic components are observed in SST signals in the Arabian Sea, Bay of Bengal and South Indian Ocean, and at the same time the Lyapunov exponent is positive for all these cases (Sect. 5). Since, sometimes Lyapunov exponent cannot distinguish between chaos and noise (Dammig and Mitschke 1993), we need to confirm that the Lyapunov exponent is positive due to nonlinearity and not noise in the present cases.

We incisively separate the periodic component and the noise component from the SST series and explore the presence of nonlinearity as follows. (a) First the periodic component is removed from the original SST signal using SVD and a residual series is created (Kanjilal et al. 1997). An $m \times n$ matrix $\boldsymbol{A}$ is formed as in Sect. 6.2 from the SST series; the number of columns (n) of $\boldsymbol{A}$ is considered as 12, since 12 is a periodicity of the SST signals in the Arabian Sea, Bay of Bengal and South Indian Ocean. SVD is performed on $\boldsymbol{A}$ to get $\boldsymbol{U}$, $\boldsymbol{S}$ and $\boldsymbol{V}$ such that $\boldsymbol{A} = \boldsymbol{USV}^{\mathrm{T}}$. The most

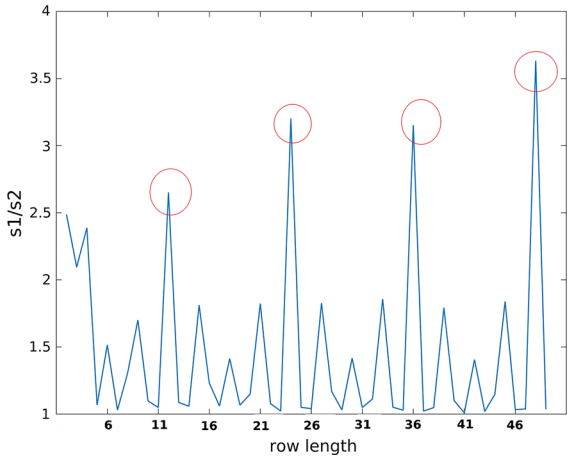

Figure 13
Periodicity spectrum of SST in the Bay of Bengal

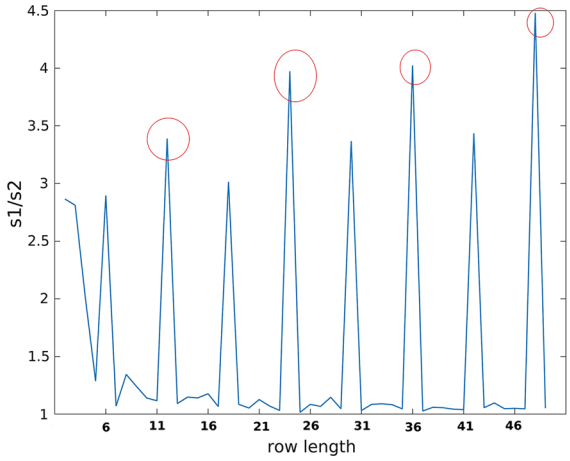

Figure 14
Periodicity spectrum of SST in the South Indian Ocean

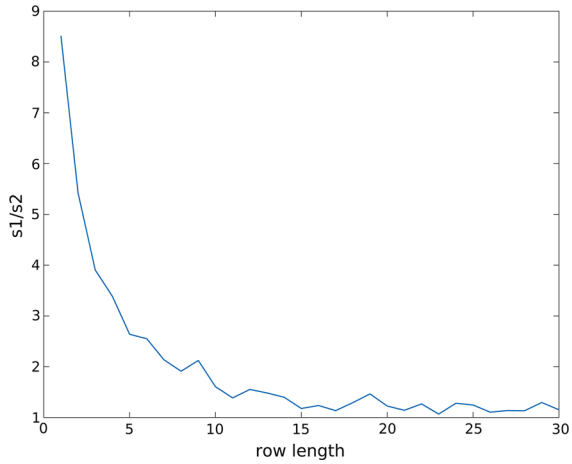

Figure 15
Periodicity spectrum of Nino 3.4 index

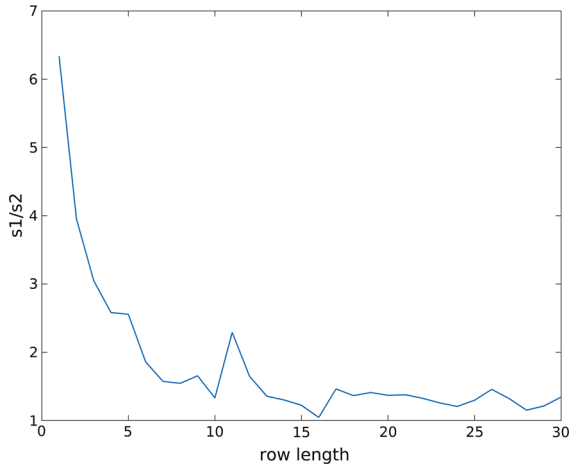

Figure 16
Periodicity spectrum of Dipole Mode index

dominant periodic component present in **A** is given by $U1\boldsymbol{S}(1,1)V1^{\mathrm{T}}$, where $U1$ is the first column of $\boldsymbol{U}$, $V1^{\mathrm{T}}$ is the first row of $\boldsymbol{V}^{T}$ and $\boldsymbol{S}(1,1)$is the largest singular value. This matrix is subtracted from $\boldsymbol{A}$ to get a residual matrix $\boldsymbol{R}$. Since the first row of $\boldsymbol{V}^{\mathrm{T}}$ represents the periodicity, subtracting the matrix $U1\boldsymbol{S}(1,1)V1^{\mathrm{T}}$ should eliminate the periodic component of the signal. So the residual time series r formed from the successive rows of $\boldsymbol{R}$ should not contain any periodicity of length 12, and is expected to consist of only nonlinear components and noise. (b) The Periodicity spectrum of this residual series is computed; for the Bay of Bengal SST series Fig. 17 show that there are no peaks in the Periodicity spectrum, confirming absence of any periodic component in the residual series. (c) The state space diagram of the residual series r (Fig. 18a) show no distinct structure and hence the residual series can be either purely noise or a combination of nonlinear component and noise. (d) Next, noise is eliminated from the residual series as follows. A Hankel matrix $\boldsymbol{H}1$ is formed with this residual series with row length of 12. SVD on $\boldsymbol{H}1$ yields $\boldsymbol{H}1=\boldsymbol{U}'\boldsymbol{S}v\boldsymbol{V}'^{T}$. In each of the above three cases, the series of column elements in $\boldsymbol{U}'$ do not show any periodicity. The insignificant last few singular values are eliminated to reconstruct the apparently noise-free signal (say, $R1$) using 6 singular values. (e) The state

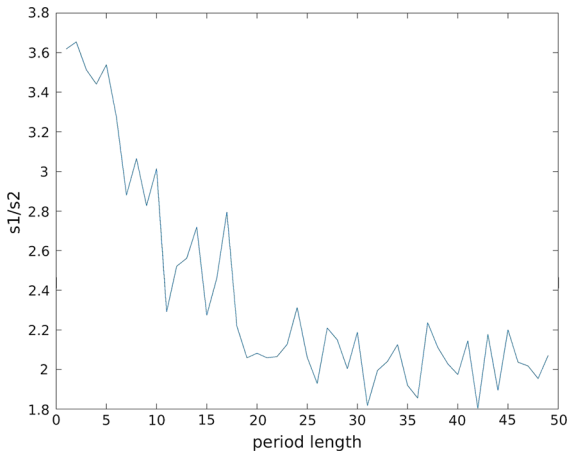

Figure 17
Periodicity spectrum of the residual series in the Bay of Bengal

space diagram is generated from $R1$ (Fig. 18b), which tends to show nonlinear characteristic. (f) To refine the residual series $R1$ further by additional elimination of noise, iterative SVD is performed, i.e. step (d) is repeated: a Hankel matrix $\boldsymbol{H}2$ is configured from $R1$ and SVD is performed on it to get $\boldsymbol{H}2= \boldsymbol{U}''\boldsymbol{S}''\boldsymbol{V}''^{\mathbf{T}}$. In this case also the columns of $\boldsymbol{U}''$ do not show any periodicity. The last few singular values of S'' are eliminated to reconstruct the signal, say $R2$, using 3 singular values. As discussed in Sect. 5, this method does not remove noise completely. Yet it helps in revealing the nonlinear component. Since the first few orthogonal modes are considered after performing SVD, noise is partially removed in this technique. (g) The state space diagram reconstructed from $R2$ (Fig. 18c) show distinct nonlinear characteristic of the Bay of Bengal SST series. The results are similar for the other two cases. The Lyapunov exponent of the filtered signal $R2$ is 0.3 for all of three cases. Since state space reconstruction is possible and the Lyapunov exponent is positive, the filtered signal $R2$ is definitely not noise, leading to the conclusion that it represents nonlinearity in the studied SST series.

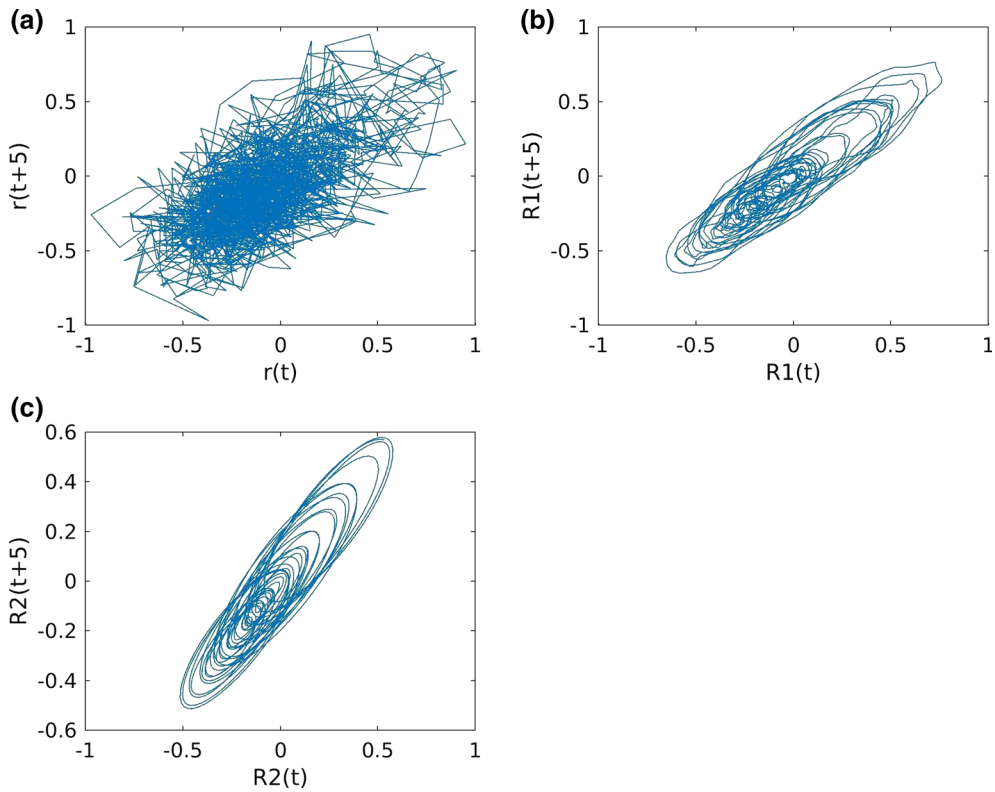

Figure 18
a Reconstructed state space figure from noisy residual series, **b** Reconstructed state space figure from filtered residual series $R1$, **c** Reconstructed state space figure from filtered residual series $R2$

7. Discussion and Conclusions

ENSO follows a similar pattern of developing during boreal summer and peaking during boreal winter. Such seasonal synchronization is a defining characteristic of ENSO. Our results contrasts with Stein et al., 2014 in which it was concluded that annual modulation of the coupled stability of the equatorial Pacific ocean–atmosphere is the mechanism which generates the synchronization of ENSO events to the annual cycle. For examining ENSO-annual cycle synchronization through phase locking, they considered a model that is similar to periodic forcing Van der Pol oscillator. In their study, chaotic oscillators were not found within the parameter space of the Van der Pol oscillator relevant to the observed ENSO. The reason is that they focused on the synchronization of ENSO, ignoring many complex features of ENSO. Their work was limited to the solutions of the Van der Pol equation which could be applicable to the seasonal synchronization of ENSO. Moreover, their model was not offered as a particularly realistic representation of ENSO, but as a system that showed similar global behavior to the simple and intermediate models of ENSO on which the frequency locking scenario was prioritized. In the model equation, they ignored the interaction of the seasonally varying growth rate and the nonlinear saturation term in the system. The interaction between the mean damping rate, the strength of the nonlinearity, the strength of the periodic forcing and the variance of the stochastic forcing was not considered in their study. If more complex aspects of ENSO was considered, the complexity of model would increase.

One of the key results of this study is to show that SST signals are chaotic in the Indian Ocean. Several studies have discussed various reason for the variability of SST in the Indian Ocean (Behera and Yamagata 2001; Waliser et al. 2003; Jochum and Murtugudde 2005). However, no quantitative analysis is performed yet in the Indian Ocean SST to show its nonlinearity. We have extracted the nonlinear component of the SST signals in the Indian Ocean. Chaotic model of El Niño has already been proposed in the literature (Tziperman et al. 1994; Stone et al.1998). Trenberth (1997) computed histograms of two El Niño indices for the period of January 1950–March 1997 and pointed out that the Nino 3 index is ''strongly'' positively skewed. Hannachi et al. 2003 showed that Nino-3 anomalies are significantly non-normal due to the presence of positive skewness. However, it has been shown that deviations from Gaussianity can be generated even in absence of slow nonlinearity (Sura et al. 2005; Martinez-Villalobos et al. 2018). We reinforce the chaotic nature of El Niño by using Singular spectrum analysis. Our analysis shows positive Lyapunov exponent, which is a confirmatory indication of chaos. Majumder et al. 2019 has shown the chaotic characteristics of IOD by reconstructing its state space diagram and showing positive Lyapunov exponent. In this study, this fact is further supported by the absence of any embedded globally stable periodic component as detected by the Periodicity spectrum analysis, which is the reason behind the uncertainty in the prediction of El Niño and IOD events.

In the present context, a signal is a mixture of periodic, nonlinear and noisy components; it is the distribution of the energy in these components that determine the nature of the composite SST signal. In this study, we are trying to address this fundamental issue. This issue is important as it is concerned with the predictability of the signal. Here we studied two broad types of signals: (1) signals in the Arabian Sea, Bay of Bengal and South Indian Ocean and (2) signals in the El Niño and IOD region. Both of these are chaotic but the first type of the signal is predictable and the second type is not easily predictable. Our analysis shows that there exists strong periodic component for first case, whereas for the second case, no periodicity is found. In the Arabian Sea and Bay of Bengal, periodic components contribute to the 61–62% variability of the signal. In the South Indian Ocean, periodic components contribute to 70% variability of the signal. Although Lyapunov exponent is mildly positive for these signals, presence of a dominant periodicity makes these series more predictable. For El Niño and IOD signals, absence of a periodic component makes the series difficult to predict. This explains why the dynamical systems of El Niño and IOD are much more complex and unpredictable compared to the other regions.

Acknowledgements

Swarnali Majumder would like to thank Director of INCOIS for supporting this work and Department of Science and Technology, Government of India for financial support vide reference no. SR/WOS-A/EA3/2016 under Women Scientist Scheme to carry out this work. The authors thank Mr. N. Kiran Kumar for the graphics. The valuable comments and suggestions by the anonymous reviewers are thankfully acknowledged.

References

Alexander, M. A., & Scott, J. D. (2008). The role of Ekman ocean heat transport in the Northern Hemisphere response to ENSO. *Journal of Climate, 21*(21), 5688–5707.

Anderson, D. (1999). Extremes in the Indian Ocean. *Nature, 401*(6751), 337–338.

Behera, S. K., & Yamagata, T. (2001). Subtropical SST dipole events in the southern Indian Ocean. *Geophysical Research Letters, 28*(2), 327–330.

Broomhead, D. S., & King, G. P. (1986). Extracting qualitative dynamics from experimental data. *Physica D: Nonlinear Phenomena, 20*(2–3), 217–236.

Casdagli, M., Eubank, S., Farmer, J. D., & Gibson, J. (1991). State space reconstruction in the presence of noise. *Physica D: Nonlinear Phenomena, 51*(1–3), 52–98.

Cattell, R. B. (1966). The scree test for the number of factors. *Multivariate Behavioral Research, 1*(2), 245–276.

Chen, C., Cane, M. A., Henderson, N., Lee, D. E., Chapman, D., Kondrashov, D., et al. (2016). Diversity, nonlinearity, seasonality, and memory effect in ENSO simulation and prediction using empirical model reduction. *Journal of Climate, 29,* 1809–1830.

Clarke, A. J. (2008). *An introduction to the dynamics of El Nino and the Southern Oscillation*. London: Elsevier Academic Press.

Dammig, M., & Mitschke, F. (1993). Estimation of Lyapunov exponents from time series: The stochastic case. *Physics Letters A, 178*(5–6), 385–394.

Deser, C., Alexander, M. A., Xie, S. P., & Phillips, A. S. (2010). Sea surface temperature variability: Patterns and mechanisms. *Annual Review of Marine Science, 2*(1), 115–143.

Dommenget, D. (2007). Evaluating EOF modes against a stochastic null hypothesis. *Climate Dynamics, 28*(5), 517–531.

Dommenget, D., & Latif, M. (2002). A cautionary note on the interpretation of EOFs. *Journal of Climate, 15*(2), 216–225.

Eckmann, J.-P., & Ruelle, D. (1992). Fundamental limitations for estimating dimensions and Lyapunov exponents in dynamical systems. *Physica D: Nonlinear Phenomena, 56*(2–3), 185–187.

Golyandina, N., Nekrutkin, V., & Zhigljavsky, A. (2001). *Analysis of time series structure: SSA and related techniques*. Boca Raton: Chapman & Hall/CRC.

Hannachi, A., Jolliffe, I. T., & Stephenson, D. B. (2007). Empirical orthogonal functions and related techniques in atmospheric science: A review. *International Journal of Climatology, 27*(9), 1119–1152.

Hannachi, A., Stephenson, D. B., & Sperber, K. R. (2003). Probablity based method for quantifying nonlinearity in the ENSO. *Climate Dynamics, 20*(2–3), 241–256.

Hegger, R., & Kantz, H. (1999). Practical implementation of nonlinear time series methods: The TISEAN package. *Chaos, 9*(2), 413–435.

http://www.cpc.ncep.noaa.gov/products/analysis_monitoring/ensostuff/ensoyears.shtml. Accessed 20 Feb 2019.

http://www.jamstec.go.jp/frcgc/research/d1/iod/HTML/Dipole%20Mode%20Index.html. Accessed 20 Feb 2019.

http://www.metoffice.gov.uk/hadobs/hadisst/. Accessed 20 Feb 2019.

Huang, B., Banzon, V. F., Freeman, E., Lawrimore, J., Liu, W., Peterson, T. C., et al. (2014). Extended reconstructed sea surface temperature version 4 (ERSST.v4): Part I. Upgrades and intercomparisons. *Journal of Climate, 28*(3), 911–930.

Jin, E. K., KinterIII, J. L., Wang, B., Park, C. K., Kang, I. S., Kirtman, B. P., et al. (2008). Current status of ENSO prediction skill in coupled ocean–atmosphere models. *Climate Dynamics, 31*(6), 647–664.

Jochum, M., & Murtugudde, R. (2005). Internal variability of Indian Ocean SST. *Journal of Climate, 18*(18), 3726–3738.

Jolliffe, I. T. (2002). *Principal component analysis* (2nd ed.). New York: Springer.

Kanjilal, P. P. (1995). *Adaptive prediction and predictive control*. London: Peter Peregrinus.

Kanjila, P. P., Palit, S., & Saha, G. (1997). Fetal ECG extraction from single-channel maternal ECG using singular value decomposition. *IEEE Transactions on Biomedical Engineering, 44*(1), 51–59.

Kanjilal, P. P., Bhattacharya, J., & Saha, G. (1999). Robust method for periodicity detection and characterization of irregular cyclical series in terms of embedded periodic components. *Physical Review E, 59*(4), 4013–4025.

Kleeman, R., & Moore, A. M. (1997). A theory for the limitation of ENSO predictability due to stochastic atmospheric transients. *Journal of Atmospheric Science, 54,* 753–767.

Kondragunta, C. R., & Gruber, A. (1997). Intercomparison of spatial and temporal variability of various precipitation estimates. *Advances in Space Research, 19*(3), 457–460.

Li, G., & Xie, S. P. (2012). Origins of tropical-wide SST biases in CMIP multi-model ensembles. *Geophysical Research Letter, 39*(22), L22703.

Majumder, S., Balakrishnan, T. M. N., & Kiran Kumar, N. (2019). Reconstruction of state space figure of Indian Ocean Dipole. In J. Bansal, K. Das, A. Nagar, K. Deep, & A. Ojha (Eds.), *Soft Computing for Problem Solving. Advances in Intelligent Systems and Computing* (Vol. 816, pp. 471–482). Singapore: Springer.

Martinez-Villalobos, C., Vimont, D. J., Penland, C., Newman, M., & Neelin, J. D. (2018). Calculating state-dependent noise in a linear inverse model framework. *Journal of Atmospheric Science, 75,* 479–496.

Munnich, M., Cane, M. A., & Zebiak, S. E. (1991). A study of self-excited oscillations of the tropical ocean–atmosphere system.

Journal of Atmospheric Sciences. Part II: Nonlinear cases, 48(10), 1238–1248.

Neelin, J. D., Battisti, D. S., Hirst, A. C., Jin, F. F., Wakata, Y., Yamagata, T., et al. (1998). ENSO theory. *Journal of Geophysical Research, 103*(C7), 14261–14290.

Newman, M., & Sardeshmukh, P. D. (2017). Are we near the predictability limit of tropical Indo-Pacific sea surface temperatures? *Geophysical Research Letters, 44,* 8520–8529.

Penland, C. (1996). A stochastic model of IndoPacific sea surface temperature anomalies. *Physica D: Nonlinear Phenomena, 98*(2), 534–558.

Penland, C., & Sardeshmukh, P. D. (1995). The optimal growth of tropical sea surface temperature anomalies. *Journal of Climate, 8,* 1999–2024.

Plaut, G., & Vautard, R. (1994). Spells of low-frequency oscillations and weather regimes in the northern hemisphere. *Journal of the Atmospheric Sciences, 51*(2), 210–236.

Rao, R. R., & Sivakumar, R. (2000). Seasonal variability of near-surface thermal structure and heat budget of the mixed layer of the tropical Indian Ocean from a new global ocean temperature climatology. *Journal of Geophysical Research, 105*(C1), 995–1015.

Rayner, N. A., Parker, D. E., Horton, E. B., Folland, C. K., Alexander, L. V., Rowell, D. P., et al. (2003). Global analyses of sea surface temperature, sea ice, and night marine air temperature since the late nineteenth century. *Journal of Geophysical Research, 108*(D14), 4407.

Rosenstein, M. T., Collins, J. J., & De Luca, C. J. (1993). A practical method for calculating largest Lyapunov exponents from small data sets. *Physica D: Nonlinear Phenomena, 65*(1–2), 117–134.

Saji, N. H., Goswami, B. N., Vinaychandran, P. N., & Yamagata, T. (1999). A dipole mode in the tropical Indian Ocean. *Nature, 401*(6751), 360–363.

Sarachik, E. S., & Cane, M. A. (2010). *The El Niño–southern oscillation phenomenon*. Cambridge, London: Cambridge University Press.

Shi, L., Hendon, H. H., Alves, O., Luo, J. J., Balmaseda, M., & Anderson, D. (2012). How Predictable is Indian Ocean Dipole? *Monthly Weather Review, 140*(12), 3867–3884.

Stein, K., Timmermann, A., Schneider, N., Jin, F., & Stuecker, M. F. (2014). ENSO seasonal synchronization theory. *Journal of Climate, 27,* 5285–5310.

Stone, L., Saparin, P. I., Huppert, A., & Price, C. (1998). El Nino Chaos: the role of stochastic resonance on the ENSO Cycle. *Geophysical Research Letters, 25*(2), 175–178.

Sura, P., Newman, M., Penland, C., & Sardeshmukh, P. (2005). Multiplicative noise and non-gaussianity: a paradigm for atmospheric regimes? *Journal of Atmospheric Science, 62,* 1391–1409.

Takens, F. (1981). Detecting strange attractors in turbulence. In D. A. Rand & L. S. Young (Eds.), *Lecture notes in mathematics* (Vol. 898, pp. 366–381). Berlin: Springer.

Thompson, C. J., & Battisti, D. S. (2000). A linear stochastic dynamical model of ENSO. *Journal of Climate. Part I: model development, 13*(15), 2818–2832.

Tourre, Y. M., & White, W. B. (1995). ENSO signals in global upper-ocean temperature. *Journal of Physical Oceanography, 25*(6), 1317–1332.

Trenberth, K. E. (1997). The definition of El Nino. *Bulletin of American Meteorological Society, 78*(12), 2771–2777.

Tziperman, E., Stone, L., Cane, M. A., & Carosh, H. (1994). El Nino chaos: overlapping of resonances between the seasonal cycle and the Pacific ocean–atmosphere oscillator. *Science, 264*(5155), 72–74.

Waliser, D. E., Murtugudde, R., & Lucas, L. E. (2003). Indo-Pacific Ocean response to atmospheric intraseasonal variability: 1. Austral summer and the Madden–Julian oscillation. *Journal of Geophysical Research, 108*(C5), 3160.

Yamagata, T., Behera, S. K., Luo, J. J., Masson, S., Jury, M., & Rao, S. A. (2004). Coupled ocean–atmosphere variability in the tropical Indian Ocean. In C. Wang, S. P. Xie, & J. A. Carton (Eds.), *Earth climate: the ocean–atmosphere interaction, geophysical monograph series* (Vol. 147, pp. 189–212). Washington: American Geophysical Union.

Yiou, P., Baert, E., & Loutre, M. F. (1996). Spectral analysis of climate data. *Surveys in Geophysics, 17*(6), 619–663.

Yu, Y., Mu, M., Duan, W., & Gong, T. (2012). Contribution of the location and spatial pattern of initial error to uncertainties in El Niño predictions. *Journal of Geophysical Research, 117*(C6), C06018.

(Received February 5, 2018, revised January 30, 2019, accepted February 18, 2019, Published online February 27, 2019)